

GRB Energetics in the Swift Era

Daniel Kocevski ¹, Nathaniel Butler ¹

kocevski@berkeley.edu, nat@astro.berkeley.edu

ABSTRACT

We examine the rest frame energetics of 76 gamma-ray bursts (GRBs) with known redshift that were detected by the Swift spacecraft and monitored by the satellite's X-ray Telescope (XRT). Using the bolometric fluence values estimated in Butler et al. (2007) and the last XRT observation for each event, we set a lower limit to their collimation corrected energy E_γ and find that a 68% of our sample are at high enough redshift and/or low enough fluence to accommodate a jet break occurring beyond the last XRT observation and still be consistent with the pre-Swift E_γ distribution for long GRBs. We find that relatively few of the X-ray light curves for the remaining events show evidence for late-time decay slopes that are consistent with that expected from post jet break emission. The breaks in the X-ray light curves that do exist tend to be shallower and occur earlier than the breaks previously observed in optical light curves, yielding a E_γ distribution that is far lower than the pre-Swift distribution. If these early X-ray breaks are not due to jet effects, then a small but significant fraction of our sample have lower limits to their collimation corrected energy that place them well above the pre-Swift E_γ distribution. Either scenario would necessitate a much wider post-Swift E_γ distribution for long cosmological GRBs compared to the narrow standard energy deduced from pre-Swift observations. We note that almost all of the pre-Swift E_γ estimates come from jet breaks detected in the optical whereas our sample is limited entirely to X-ray wavelengths, furthering the suggestion that the assumed achromaticity of jet breaks may not extend to high energies.

Subject headings: gamma-rays bursts—

¹Astronomy Department, University of California, 601 Campbell Hall, Berkeley, CA 94720

1. Introduction

As of June 2007, the Swift spacecraft’s Burst Alert Telescope (BAT) (Gehrels et al. 2004; Barthelmy et al. 2005b) had detected over 200 gamma-ray bursts (GRBs) and has followed $> 80\%$ with the satellite’s X-ray Telescope (XRT) (Burrows et al. 2005a). The data that has accumulated as a result of the huge success of the XRT has shown that the X-ray light curves of GRB afterglows are far more complex than previous observations (e.g., Frontera et al. 2000; Gendre et al. 2006) had indicated. Large drops in the X-ray emission immediately following a GRB (Barthelmy et al. 2005a) are superseded by a shallow decay (Granot, Knigl, & Piran 2006), ultimately giving way to the late-time afterglow light curve observed by pre-Swift X-ray instruments. In many cases these light curve phases are punctuated by flaring activity occurring hundreds to thousands of seconds after the initial energy release (Burrows et al. 2005b). Yet in other cases only a single light curve phase manifests, yielding an uninterrupted power law decline that extends directly from the prompt gamma-ray emission into the X-ray regime lasting several days to weeks after the event (Schady et al. 2006; Sato et al. 2007; Mundell et al. 2007; Holland et al. 2007).

Relatively few of these XRT monitored afterglow light curves have shown properties consistent with the late-time steepening that had been observed to occur in the optical light curves of pre-Swift GRBs (Harrison et al. 1999; Stanek et al. 1999). This sharp drop in the flux of some pre-Swift afterglows has been interpreted as a sign of the deceleration and/or lateral expansion of a highly collimated relativistic outflow (Rhoads et al. 1997). The existence of such a jet structure in the GRB outflow has become an integral part of the theoretical description of these events (Mészáros 2002) and indeed a necessary component to explain the enormous amount of radiated energy inferred if the prompt emission is assumed to be isotropic (Waxman, Kulkarni, & Frail 1998; Fruchter et al. 1999).

Several authors have examined the presence, or lack thereof, of jet breaks in the X-ray afterglow light curves collected by the XRT. Burrows et al. (2007) examined the X-ray light curves of ~ 150 GRB afterglows and concluded that the “canonical” jet model behavior, consisting of an achromatic light curve break between $t_{\text{jet}} \sim 1$ to 4 days and a post-break power law decay index $F_\nu \propto t^{-\alpha}$ steeper than $\alpha = 2.0$ (Rhoads et al. 1997; Sari et al. 1999), are extremely rare. They find that many of these X-ray light curves do exhibit breaks, but that they occur at about 10^4 seconds, far earlier than the jet breaks observed at optical wavelengths of pre-Swift GRBs. These early breaks are typically followed by power law decays which are shallower than the minimum decay index predicted by simple jet models. In all, the preliminary analysis done by Burrows et al. (2007) revealed only 6 events with light curve breaks that were consistent with theoretical predictions of jet break behavior. Subsequently, Panaitescu (2007a) performed a similar analysis of 236 GRB afterglows and

found 30 events which were consistent with the behavior expected from standard jet models. He also reported an additional 27 events with potential jet breaks, for which the spectral and temporal properties were not entirely consistent with model predictions, and another 38 events which exhibit no temporal breaks in their X-ray light curves. In all, Panaitescu concludes that some 60% of well-monitored X-ray afterglows exhibit some evidence for a potential late-time jet break.

Recently, Butler et al. (2007) reported on the first comprehensive catalog of bolometric energy fluences of GRBs detected by the BAT instrument. One implication of that analysis is that a significant fraction of the Swift events with known redshift z are under-energetic relative to pre-Swift events. This is likely due to a factor 3–10 greater sensitivity and lower resulting detection threshold of the BAT, relative to previous instruments. (e.g., Barthelmy et al. 2005b). One consequence of this higher sensitivity may be a capacity to detect a greater fraction of more distant, high- z , events. Both of these effects, a lower E_{iso} and a higher z , have the effect of increasing the predicted jet break time t_{jet} given a fixed collimation angle, or more importantly, a standard collimation corrected energy E_{γ} .

In this paper, we examine the source frame energetics of 76 GRBs detected by the Swift spacecraft with known redshift. Using the bolometric fluence values estimated in Butler et al. (2007) and the last XRT observation, we calculate a lower limit E_{γ} for our entire sample to determine the fraction of Swift events that could accommodate a jet break beyond the last XRT observation and still be consistent with the relatively narrow pre-Swift E_{γ} distribution found by Frail et al. (2001) and Bloom, Frail, & Kulkarni (2003). To analyze the breaks that do exist in a subset of light curves, we employ a Bayesian blocks algorithm (Scargle 1998; Butler & Kocevski 2007) to fit the various segments of XRT light curves, allowing for an automated and robust approach at measuring break times as well as pre- and post-break power law indices in the afterglow decay. We find that the higher sensitivity of the BAT instrument allows for a large fraction, roughly $\sim 68\%$, of our sample to accommodate a jet break beyond the last XRT observation and still have an energy consistent with the pre-Swift E_{γ} distribution. We find that relatively few of the X-ray light curves for the remaining events show evidence for breaks in their X-ray light curves that are consistent with that expected from the effects of jet collimation. The application of these X-ray selected breaks, which typically occur far earlier than the pre-Swift jet breaks observed at optical wavelengths, result in an E_{γ} distribution which has a median value that is lower than that of the pre-Swift sample. We find that the energetics predicted by most of the breaks reported by Panaitescu (2007a) suffer from the same difficulties. The assumed validity of the narrowness of the pre-Swift E_{γ} distribution casts doubt on the interpretation of many of these early temporal breaks as jet breaks, unless the intrinsic spread in the collimation corrected energy is much wider than had previously been reported. We discuss our data acquisition and reduction

techniques in §2 and expand upon our results in §4. We discuss the implications of these results §5.

2. Data & Analysis

We form a sample of 76 GRBs detected by Swift with redshifts reported to the Gamma-ray bursts Coordinates Network (GCN) circulars. The entire list of bursts including redshifts and their associated references can be found on Table 1. For these, and all other Swift events, we download the BAT and XRT data products from the *Swift* Archive¹ and process the data with version 0.10.3 of the `xrtpipeline` reduction script and other tools from the HEASoft 6.0.6² software release. We employ the calibration files from the 2006-10-14 BAT database release for this analysis. The reduction from cleaned event lists output by the `xrtpipeline` code and from the HEASoft BAT software to science ready light curves and spectra is described in extensive detail in Butler & Kocevski (2007). All of our resulting BAT spectral fits and X-ray light curves to which we apply our analysis are publicly available³. The errors regions reported throughout the paper correspond to the 90% confidence interval.

2.1. BAT Spectral Fitting

A full and extensive description of the fitting methods use to estimate the bolometric fluence S_{bol} values for our sample of Swift events is discussed in detail in Butler et al. (2007), although we will briefly summarize our approach here. We traditionally fit the reduced BAT data for each event with the simplest of three possible models, consisting of a simple powerlaw, a powerlaw times an exponential cutoff, and a smoothly-connected broken powerlaw. We would then derive confidence intervals by considering random realizations of the data given the best-fit model for each model parameter constrained by the best-fit model. This approach turns out to be very limited for Swift events, due to the narrow energy bandpass of the BAT instrument. In particular it is possible to measure a νF_ν spectral peak energy $E_{\text{pk,obs}}$ for only about one third of the events in the entire Swift sample. Therefore, for this study we employ a more powerful Bayesian approach which assumes that each burst spectrum has an intrinsic spectrum containing the $E_{\text{pk,obs}}$ parameter, and we derive a prob-

¹<ftp://legacy.gsfc.nasa.gov/swift/data>

²<http://heasarc.gsfc.nasa.gov/docs/software/lheasoft/>

³<http://astro.berkeley.edu/~nat/swift>

ability distribution for that parameter given the observed data. We find that the use of prior information, in this case thousands of observations of GRBs by the BATSE instrument (Preece et al. 2000; Kaneko et al. 2006), can be exploited to derive reasonably tight limits on $E_{\text{pk,obs}}$ even for cases where $E_{\text{pk,obs}}$ is well above the detection passband. The resulting fits allow us to estimate the true bolometric burst energy fluence despite the limited bandpass of the BAT detector.

To test the validity of our measured S_{bol} and $E_{\text{pk,obs}}$ values, we compare them to values reported to the GCN circulars for 27 events which were detected by both the Swift and Konus-Wind spacecrafts (Aptekar et al. 1995) and another 7 events detected by both the Swift and Suzaku spacecrafts (Mitsuda et al. 2007). We find that our S_{bol} and $E_{\text{pk,obs}}$ values are closely consistent with the preliminary Konus-Wind and Suzaku values to within a 90% confidence limit of their reported errors. Further analysis and comparisons of our S_{bol} and $E_{\text{pk,obs}}$ measurements with other instruments for a sample of 216 Swift detected GRBs can be found in Butler et al. (2007). The final conclusions drawn from that analysis indicates that there is no bias in either the $E_{\text{pk,obs}}$ or S_{bol} measurements produced through our Bayesian approach, allowing for a correct bolometric accounting of the total isotropic and/or collimation-correction energy emitted by these events.

2.2. X-ray Light Curve Region Selection and Fitting

In order to measure the temporal power-law indices $F_\nu \propto t^{-\alpha}$ of separate segments in the X-ray light curve, we fit the X-ray light curve data using an extension of the Bayesian blocks algorithm (Scargle 1998) to piecewise logarithmic data. Developed in Butler & Kocevski (2007), the algorithm determines the most likely multi-segment power law fit consistent with the light curves, without the need for human intervention. The final result of the fitting routine for a sample of events can be seen in Figure 1, where individual light curve segments have been automatically determined and fit to power-laws of various indices¹. For each break, we record the time of occurrence along with the pre- and post-break power law indices, α_1 and α_2 . The time of the last 3σ detection t_{XRT} of the source by the XRT is also recorded for each event, although this determination does not depend on the Bayesian block algorithm. The pre- and post-break α , the time of the break, and t_{XRT} are listed in Tables 1 & 2, where available.

¹Similar light curves are available for all Swift bursts at <http://astro.berkeley.edu/~nat/swift>

2.3. Isotropic and Collimation Corrected Energy Calculations

We calculate the total isotropic equivalent energy E_{iso} emitted by the GRB from the measured fluence S_{bol} through the standard equation

$$E_{\text{iso}} = \frac{4\pi D_l^2}{1+z} S_{\text{bol}} k \quad (1)$$

where D_l is the luminosity distance at redshift z and k represents the multiplicative factor or order unity that translates the bandpass of the detector in the observer frame to a standard rest-frame bandpass, here chosen to be $1 - 10^4$ keV (Bloom, Frail, & Sari 2001). We employ the method outlined in Amati et al. (2002) to calculate k . For the case of a homogeneous circumburst medium Sari et al. (1999), the observed jet break time t_{jet} is related to the jet opening angle θ_{jet} through

$$\theta_{\text{jet}} = 0.101 \text{ rad} \left(\frac{t_{\text{jet}}}{1 \text{ day}} \right)^{3/8} \left(\frac{\xi}{0.2} \right)^{1/8} \left(\frac{n}{10 \text{ cm}^{-3}} \right)^{1/8} \left(\frac{1+z}{2} \right)^{-3/8} \left(\frac{E_{\text{iso}}}{10^{53} \text{ ergs}} \right)^{-1/8} \quad (2)$$

where ξ represents the efficiency of converting the blast wave’s kinetic energy into gamma-rays and n is the circumburst density. Throughout our analysis, we have chosen to assume a fixed value for both the efficiency and density parameters, using $\xi = 0.5$ and $n = 3.0$ (Granot, Knigl, & Piran 2006; Kumar et al. 2007). Although, varying these assumptions within reasonable ranges ($\xi = 0.1 - 1.0$ and $n = 3.0 - 30$) has little effect on our final results. The conversion from E_{iso} to the collimation corrected energy E_γ is then a simple geometric correction given by

$$E_\gamma = E_{\text{iso}} (1 - \cos \theta_{\text{jet}}) \quad (3)$$

We assume a cosmology with $h = 0.71$, $\Omega_m = 0.3$, and $\Omega_\Lambda = 0.7$ throughout.

3. Results

The redshift distribution of all 76 GRBs detected by Swift in comparison to the 48 pre-Swift GRBs Friedman & Bloom (2005) is shown in Figure 2. The median redshift of the Swift detected events is $z = 1.8$ with a standard deviation σ of 1.59 compared to the median pre-Swift redshift of $z = 1.1$ and σ of 0.98. A Kolmogorov-Smirnov (K-S) analysis gives the associated probability that the two distributions are consistent to be exceedingly small, at $p = 0.015$.

For the purposes of comparing our E_{iso} , and eventually E_γ , estimates to those of pre-Swift GRBs with known redshift, which consist almost exclusively of long duration events,

we form a subset of long bursts (LB) from our original sample of 76 Swift GRBs. For this set we exclude 9 events which have been classified as short bursts ($t_{90} \lesssim 2$ sec), another 3 events which are peculiarly under-luminous (XRF 060218, GRB GRB 050826, GRB GRB 051109B) and 1 event (GRB 060124) for insufficient BAT coverage during the prompt emission (see Butler et al. (2007) for more details), leaving a total of 63 LB events. A plot of E_{iso} vs. redshift for all detected pre-Swift (red) and post-Swift (blue) events (Long, Short, and SN-associated GRBs) is shown in Figure 5.

The distribution of E_{iso} for the Swift detected GRBs marginally extends to lower energies compared to the pre-Swift sample, even after the admittedly ad hoc exclusion of peculiarly under-luminous events. The median E_{iso} value of the Swift sample is roughly $4.11^{+2.53}_{-0.54} \times 10^{52}$ erg compared to $7.76^{+0.01}_{-1.29} \times 10^{52}$ erg for the pre-Swift sample. A K-S test returns a probability of $p = 0.093$. The inclusion of the under-luminous LB events only worsens the disparity between the two samples.

How does the observed increase in the median redshift and the decrease in the median E_{iso} of the Swift selected sample effect where we should expect to observe jet breaks in the XRT data? From Equations 2 and 3 we can see that

$$t_{\text{jet}} \approx 452 \left(\frac{\xi}{0.2} \right)^{-1/3} \left(\frac{n}{10} \right)^{-1/3} \frac{1+z}{2} \left(\frac{E_{\text{iso}}}{10^{53} \text{ ergs}} \right)^{-1/8} \left[\cos^{-1} \left(1 - \frac{E_{\gamma}}{E_{\text{iso}}} \right) \right]^{8/3} \text{ days} \quad (4)$$

Given a fixed E_{γ} , both effects should increase the observed delay between the initial explosion and the subsequent steepening of the afterglow light curve. There is sufficient evidence from pre-Swift observations to suggest that E_{γ} has a narrow range of values for typical long GRBs. Using the measured t_{jet} , E_{iso} , and z for a sample of 17 bursts, Frail et al. (2001) and later Bloom, Frail, & Kulkarni (2003) concluded that this geometrically corrected energy is narrowly clustered around a standard energy, which Bloom, Frail, & Kulkarni (2003) report as $E_{\gamma} = 1.33 \times 10^{51}$ ergs with a variance of 0.35 dex. Assuming this pre-Swift determined value, and its variance, we can calculate the expected t_{jet} distribution for our Swift detected sample.

A histogram of the ratio between this expected t_{jet} and the last 3σ XRT observation t_{XRT} is shown Figure 4. Most events, when assuming a fixed E_{γ} , have an expected t_{jet} that is near or beyond the last significant XRT detection. The median expected \bar{t}_{jet} is 10.37 days after the GRB, leading to 63% of our LB sample to have an expected t_{jet} that occurs beyond the last 3σ XRT detection. Three events in our LB subset were excluded from this analysis because their E_{iso} values were below 1.33×10^{51} ergs and therefore could not accommodate an E_{γ} that was consistent with the pre-Swift energetics distribution. Such a high ratio of events with $t_{\text{jet}} > t_{\text{XRT}}$ is somewhat surprising, given that the median duration of XRT observations is typically an order of magnitude longer than the pre-Swift t_{jet} distribution. A comparison

of t_{XRT} for our LB sample to the pre-Swift t_{jet} is shown in Figure 5, with the pre-Swift jet breaks shown as the filled histogram. The median of the two distributions differ by roughly an order of magnitude.

What of the light curve breaks that do exist in our LB sample? Of the 20 GRBs, or $\sim 37\%$ of our sample, for which the expected $t_{\text{jet}} < t_{\text{XRT}}$, only 3 were determined by Panaitescu (2007a) to have jet breaks that are consistent with the standard jet model, 5 events were classified as containing potential jet breaks, and 4 events showed no evidence for late-time breaks in their light curve. The remaining events in this subset have insufficient coverage to test for the existence of jet breaks. Of these 8 events that do show some steepening in their light curves, all have breaks that occur earlier than the expected t_{jet} , indicating that their E_γ values must be lower than the assumed standard energy determined from pre-Swift GRBs. Of the 43 GRBs, or $\sim 63\%$ of our sample, for which the expected $t_{\text{jet}} > t_{\text{XRT}}$, 8 were determined by Panaitescu (2007a) to have jet breaks that are consistent with the standard jet model, 3 events containing potential jet breaks. For these 11 events with some sign of steepening, their interpretation as jet breaks will necessarily yield E_γ values that are far less than the narrow peak of the pre-Swift E_γ distribution because their expected t_{jet} is greater than the last XRT observation.

We examine the E_γ distribution resulting from the use of these early light curve breaks as potential jet breaks, regardless of their predicted t_{jet} , to compare this distribution to the pre-Swift E_γ distributions found by Frail et al. (2001) and Bloom, Frail, & Kulkarni (2003). We do this by utilizing the 25 GRBs in our sample that overlap with the GRBs examined by Panaitescu (2007a). In this subset, 13 events with redshift were determined to harbor breaks consistent with the standard jet models, and another 12 with “potential” jet breaks. Neither the jet break time or the pre- or post-break decay indices were reported by Panaitescu (2007a) for the events with “potential” jet breaks, so we utilize the Bayesian blocks algorithm described in §2.2 to measure all three quantities. The resulting fit parameters are displayed in Table 2.

The resulting post-Swift E_γ distribution in comparison to the pre-Swift distribution is shown in Figure 6. The median of the post-Swift distribution, as determined through the use of all 25 GRBs, is roughly 9.0×10^{49} ergs with a variance of 0.90 dex. The median jet break time for the entire sample is $\log t_{\text{jet}} \sim 4.73$ days. The peak of the post-Swift E_γ distribution is much broader and roughly an order of magnitude lower than the distribution derived from the pre-Swift observations. A K-S test returns a probability of $p = 5.66 \times 10^{-3}$ that the pre-Swift and post-Swift distributions are drawn from the same parent population. The lower and upper limits on E_γ for all events which show no sign of any breaks in their afterglow light curves are represented as vertical bars in Figure 6. The last 3σ detection of the XRT

sets the lower bound whereas the upper bound is set to equal the burst’s isotropic equivalent energy E_{iso} . In contrast to the 25 events with breaks in their light curves, the events with no breaks begin to push the post-Swift E_γ distribution to higher energies in comparison to the pre-Swift distribution. Two significant outliers (GRB 050820A and GRB 061007) in particular have resulting lower limits to their energies that are above 10^{52} ergs.

4. Discussion

The results presented in the previous section paint a complicated picture for GRB energetics in the Swift era. The combination of more distant events and a wider distribution in the observed isotropic equivalent energy has resulted in a much broader E_γ distribution for Swift detected GRBs. The breaks that do exist in the X-ray light curves of many events are typically inconsistent with standard jet model predictions and occur earlier than the pre-Swift jet break distribution. Their application as jet breaks yields an under-luminous E_γ distribution that is highly inconsistent with the pre-Swift sample.

It may be the case, as also suggested by Panaitescu (2007a), that a significant fraction of these potential jet breaks are actually associated with some mechanism other than jet collimation, such as the cessation of late-time energy injection (Rees & Mészáros 1998). The events which have post-break decay indices α_2 that are shallower than the -1.5 expected from standard jet models tend to have shallower breaks when compared to the rest of the sample. The median difference between the pre and post-break decay indices for these bursts is roughly $\Delta\alpha \sim 0.48$ compared to that of bursts that have model consistent jet breaks which have $\Delta\alpha \sim 1.04$. Second, the distribution of α_2 for the events with model inconsistent jet breaks is fully consistent with the decay indices exhibited by events which have no breaks in their light curves, as shown in Figure 7. This could indicate that some of these observed breaks may be due to end of the plateau phase that has become ubiquitous in Swift X-ray light curves (Nousek et al. 2006) and that the true jet break had not been observed by the end of the XRT observations.

Liang et al. (2007) has recently completed an extensive analysis of the plateau phases observed in XRT light curves and found that the distribution of transition times to a steeper decay is centered at $\log t_b = 4.09 \pm 0.61$ seconds and that the distribution of power law indices during the phases peaks at $\alpha_1 \sim 0.35 \pm 0.35$. This is in comparison to the median jet break time of $\log t_{\text{jet}} = 4.72 \pm 0.60$ and a pre-break power law index distribution of $\alpha_1 \sim 0.82 \pm 0.23$ for model inconsistent jet break in our Swift sample. Although the distribution of pre-break decay indices is higher than the distribution of plateau decays reported by Liang et al. (2007), it may still be the case that some of the events in our sample

consist of light curves with plateau breaks which are steep enough and occur at the upper end of the t_b distribution such that they could be considered as jet breaks which do not confirm entirely to standard jet models.

If we excluding GRBs with X-ray breaks have a post-break decay indices that is shallower than $\alpha \sim 1.5$, we receive a median post-Swift $E_\gamma \sim 1.12_{-2.92}^{+0.38} \times 10^{50}$ ergs with a variance of 0.65 dex. The removal of these events eliminates the low energy tail from the post-Swift E_γ distribution, making it more consistent with the optically determined pre-Swift energetics distribution, but the distribution is still an order of magnitude lower than the E_γ distribution estimated from pre-Swift GRBs. The resulting post-Swift distribution, in comparison to the pre-Swift distribution, is shown in Figure 8. If we assume that these shallow breaks were due to some mechanism other than jet collimation and that the true jet breaks had not yet manifested by the end of the XRT observations, then we can place upper and lower limits on their collimation corrected energy. These limits are again represented as vertical bars in Figure 8. Much like the events with no detected jet breaks, the limits on E_γ for many of these shallow break events are well above the pre-Swift E_γ distribution, pushing the upper end of the post-Swift energy distribution well beyond 10^{52} ergs.

We note that all of the pre-Swift E_γ estimates that we have used in this analysis come from jet breaks detected in the optical whereas our sample is limited entirely to X-ray wavelengths. There is evidence (Panaiteescu et al. 2006; Perley et al. 2007; Curran et al. 2007; Oates et al. 2007) to suggest that the X-ray and optical emission may not evolve achromatically at late times as predicted by blast wave models (Mészáros & Rees 1997; Sari, Piran & Narayan 1998; Panaiteescu & Kumar 2000). Many of the various light curve phases observed in the X-ray do not always manifest at optical wavelengths, indicating that the X-ray and optical emission may originate from distinct and separate physical components. Such a two component model has been proposed by Kumar & Granot (2003) in which the X-ray and optical emissions originate from two distinct jets of differing degrees of collimation. This model has been invoked by Panaiteescu et al. (2006) and Oates et al. (2007) to explain breaks observed in the X-ray light curves of several events which show no such behavior at optical wavelengths. In the context of the two component jet model, the X-ray break would be due to a narrow central jet and the optical from a wider jet which presumably would cause a break at a much later time. Alternatively, Panaiteescu (2007b) has suggested that the various components in many X-ray light curves may originate from the scattering of forward shock photons by a relativistic outflow behind the leading blast wave. Under the right conditions, these boosted photons could be more luminous than the X-ray flux of the forward shock itself. In either case, all of the E_γ values determined through the use of X-ray breaks become suspect and may not reflect the overall energy budget of the GRB.

These considerations would lead to two possible, albeit conflicting, scenarios. First, that the true E_γ distribution of long GRBs is indeed narrowly clustered about a few times 10^{51} ergs as the pre-Swift optical data would suggest but that the breaks seen at X-ray wavelengths are unrelated to jet collimation. In this case, a majority of the optical breaks would have to occur well beyond ~ 1 day. We find that the median expected jet break time for the Swift sample, given a standard energy of $E_\gamma \sim 1.33 \times 10^{51}$ ergs, is roughly $t_{\text{jet}} \sim 10$ days, considerably beyond the duration, and indeed capability, of most observing campaigns. In this case, only 32% of the Swift sample with known redshift have XRT observations that extend beyond their expected t_{jet} . This scenario would then require some mechanism which could essentially mask the effects of jet collimation at X-ray wavelengths for the events which show straight power law decays to late times.

Even if we dismiss the assumption that the achromaticity of jet breaks extends to X-ray wavelengths, there still appear to be events that challenge the notion of a narrow E_γ distribution even at optical wavelengths. The well studied GRB 061007 has an expected jet break at ~ 0.18 days but yet exhibits a single power law at optical wavelengths out beyond 1 day, resulting in a lower limit of $E_\gamma \sim 1.5 \times 10^{52}$ (Schady et al. 2006). Likewise, 4 events (GRB 050416A, GRB 051016B, GRB 060428B, GRB 060512) have E_{iso} values that are below 10^{51} ergs, meaning any break in their optical light curve would make the inferred energy released by these events even more inconsistent with pre-Swift estimates.

This leads to the second scenario in which the jet breaks are indeed seen in some X-ray light curves but that long cosmological GRBs have a much wider distribution of E_γ than pre-Swift GRBs would suggest. A wider E_γ distribution has already been suggested by low energy events such as XRFs and SN-GRBs and there is no a priori reason to believe that the gamma-rays, which represent such a sub-dominate fraction of the entire energy in the collapsar model, should necessarily be standard among all events. It could then still be the case that some the breaks seen in the X-ray wavelengths could be due to jet collimation while others may be manifestation of other mechanisms that only effect the resulting X-ray emission.

In this case, the disparity between the pre- and post-Swift energetics distributions would imply a significant bias towards the detection of jet breaks in bright, relatively nearby, GRBs in the pre-Swift era. The effects of such a bias begin to be apparent in Figure 9, where E_{iso} is plotted vs. redshift for all pre- (red) and post- (blue) Swift events, including long, short, and SN-associated GRBs. The events for which jet breaks were detected in the pre-Swift sample are plotted in green and represent the brighter fraction of the distribution. Furthermore, the presence of multiple light curve breaks and the long delay between the GRB and subsequent optical and X-ray observations prior to the Swift mission may have also allowed for a bias

towards the selection of the last break in a multi-break light curve as the potential jet break. This would have essentially created an artificial lower limit on the pre-Swift E_γ distribution.

Ultimately, more contemporaneous observations at optical and X-ray wavelengths will be needed to determine which fraction of the X-ray breaks are truly achromatic. Observing more jet breaks at optical wavelengths would also allow for a direct comparison between the pre- and post-Swift energetics distribution, hopefully eliminating the ambiguity involved with using jet break times determined at different wavelengths. This will require a continued interest by the GRB community in obtaining deep optical and/or IR imaging of afterglows several days or even weeks after the initial explosion. Such observations will prove crucial in resolving many of these questions regarding the collimation and energetics of GRBs.

5. Acknowledgments

D.K. acknowledges financial supported through the NSF Astronomy & Astrophysics Postdoctoral Fellowships under award AST-0502502. N.B. gratefully acknowledges support from a Townes Fellowship at U. C. Berkeley Space Sciences Laboratory and partial support from J. Bloom and A. Filippenko.

REFERENCES

- Amati, L., A&A, 390, 81
- Aptekar et al. 1995, SSRv, 71, 265A
- Barthelmy, S. D., et al. 2005, Space Science Reviews, 120, 143
- Barthelmy, S. D., et al. 2005a, 2005, ApJ, 635L, 133
- Bloom, J., S., Frail, D., A., Sari, R. 2001, AJ, 121.2879B
- Bloom, J. S.; Frail, D. A.; Kulkarni, S. R 2003, ApJ, 594, 674B
- Burrows, D. N., et al. 2005, Space Science Reviews, 120, 165
- Burrows, D. N., et al. 2005, Science, 309, 1833
- Burrows, D. N., et al. 2007, Submitted to Philosophical Transactions (astro-ph/0701046)
- Butler, N. & Kocevski, D. 2007, ApJ, 663, 407B

- Butler, N., Kocevski, D., Bloom, J. S., Curtis, J. L. 2007, Submitted to ApJ(2007arXiv0706.1275B)
- Curran, P. A., et al. 2007, Submitted to MNRAS Letters (arXiv0706.1188C)
- Frail, D. A., et al. 2001, ApJ, 562, L55
- Friedman, A., S.; Bloom, J., S. 2005, ApJ, 627, 1F
- Frontera, F., et al. 2000, ApJSuppl., 127, 59-78
- Fruchter, A. S., et al. 1999, ApJ, 519, L13
- Gehrels, N., et al. 2004, ApJ, 611, 1005
- Gendre, B., 2006, A&A 455, 803
- Ghirlanda, G., Ghisellini, G., & Lazzati D. 2004, ApJ, 616, 331
- Granot, J., Knigl A. & Piran, T. 2006, MNRAS, 370, 1946
- Harrison, F. A., et al. 1999, ApJ, 523, L121
- Holland et al. 2007, AJ, 133, 122H
- Kaneko, Y., Preece, R., Briggs, M., S., Paciesas, W., S., Meegan, C., A.; Band, D., L. 2006, ApJS, 166, 2
- Kolaczyk, E. D., Dixon, D. D. 2000, ApJ, 534, 490K
- Kumar P., & Granot, J.,
- Kumar P. 2007, MNRAS, 376L, 57K
- Liang E., Zhang B., Zhang B., 2007, arXiv:0705.1373v2
- Massaro, F., Cutini, S., Conciatore, M. L., & Tramacere, A. 2007, in prep.
- Mészáros, P. & Rees M., 1997, ApJ, 476, 232
- Mészáros, P. 2002 ARA&A, 40, 137M
- , Mitsuda, K., et al. 2007, PASJ, 59, S1
- Mundell, C. 2007, ApJ, 660, 489M
- Nousek J. A. et al, 2006, ApJ, 642, 389

- Oates, S. R., 2007, Accepted to MNRAS (arXiv0706.0669O)
- Panaiteanu A., Kumar P., 2000, ApJ, 543, 66
- Panaiteanu, A.; Meszaros, P.; Burrows, D.; Nousek, J.; Gehrels, N.; O’Brien, P.; Willingale, R. 2006, MNRAS, 369, 2059P
- Panaiteanu, A. 2007, accepted by MNRAS (2007arXiv0705.1015P)
- Panaiteanu, A. 2007, submitted to MNRAS (2007arXiv:0708.1509v2)
- Perley, D., et al. 2007, Submitted to ApJ (astro-ph/0703538)
- Preece, R. D., Briggs, M. S., Mallozzi, R. S., Pendleton, G. N., Paciesas, W. S. 2000, ApJS, 126, 19P
- Rees, M. J., Mészáros, P., 1998, ApJ, 496, L1
- Rhoads, J. E. 1997, ApJ, 487, L1
- Sari R., Piran T., Narayan R., 1998, ApJ, 497, L17
- Sari, R., Piran, T., & Halpern, J. P. 1999, ApJ, 519, L17
- Sato, G., 2007 ApJ, 657, 359S
- Scargle, J. D. 1998, ApJ, 504, 405
- Schady, P., et al. 2006, Accepted by MNRAS (astro-ph.11081S)
- Stanek, K. Z., Garnavich, P. M., Kaluzny, J., Pych, W., & Thompson, I. 1999, ApJ, 522, L39
- Waxman, E., Kulkarni, S. R., & Frail, D. A. 1998, ApJ, 497, 288

Figures

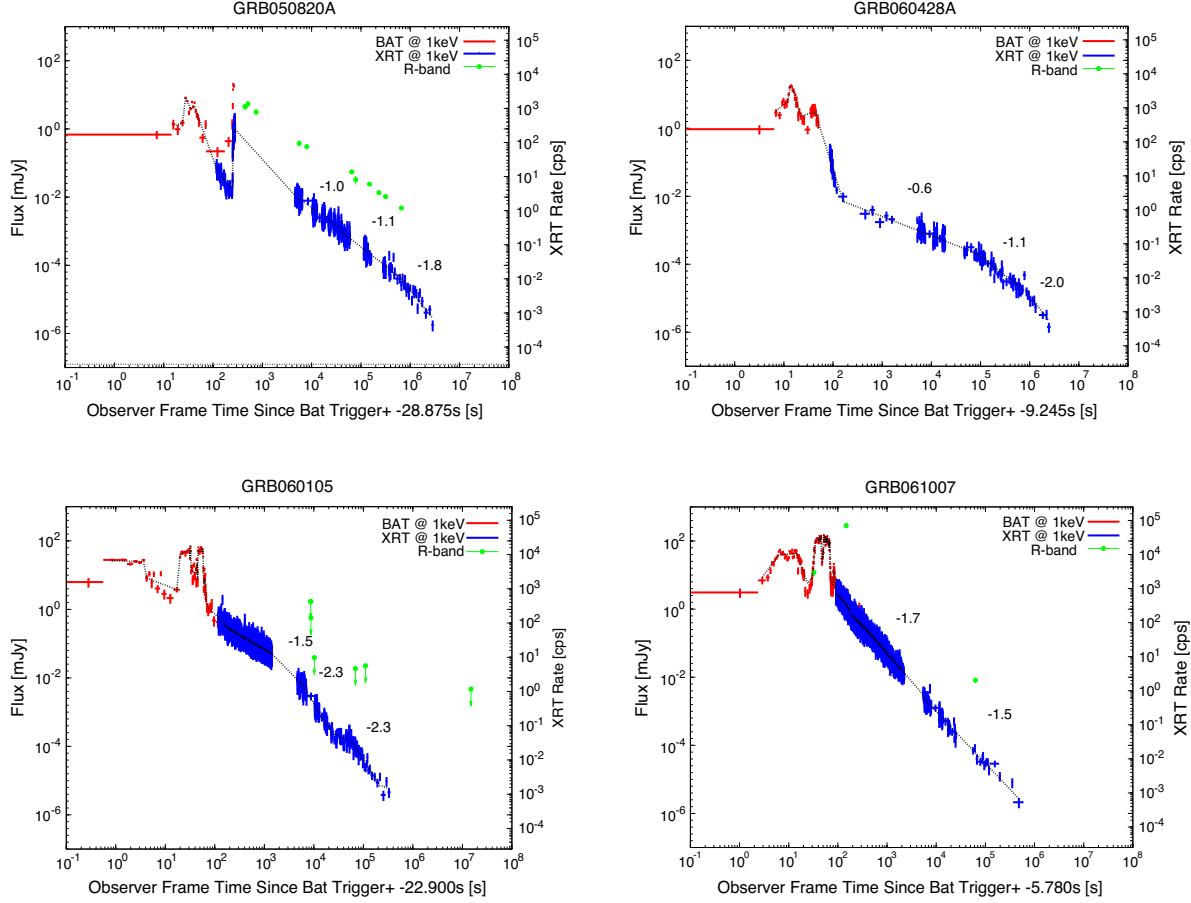


Fig. 1.— Composite BAT (red) and XRT (blue) light curves of four well sampled GRBs exhibiting a characteristic range of potential jet break behavior. GRB 050820A, GRB 050428A, and GRB 060105 have late-time breaks that are consistent with standard jet models, although GRB 050428A and GRB 060105 have multiple breaks at earlier times that can be misidentified as sudo jet breaks if the last break had not been detected. The remaining event, GRB 061007, is the quintessential example of a GRB that lacks any breaks in its afterglow light curve.

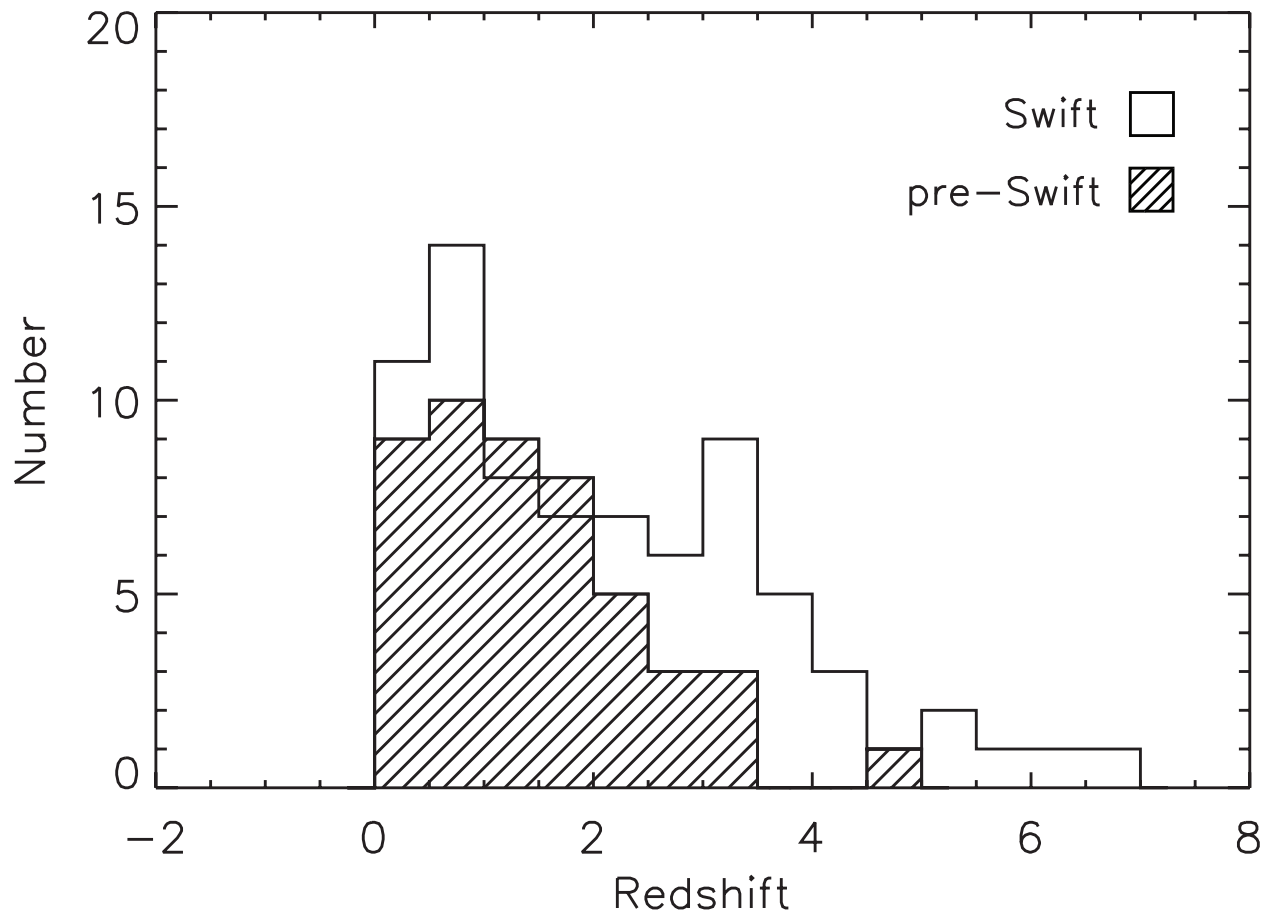


Fig. 2.— The redshift distribution of all 76 GRBs detected by Swift in comparison to the 48 pre-Swift GRBs. The median redshift of the Swift detected events is slightly higher ($z = 1.8$) than the pre-Swift distribution ($z = 1.1$), owing to the greater sensitivity of the BAT instrument.

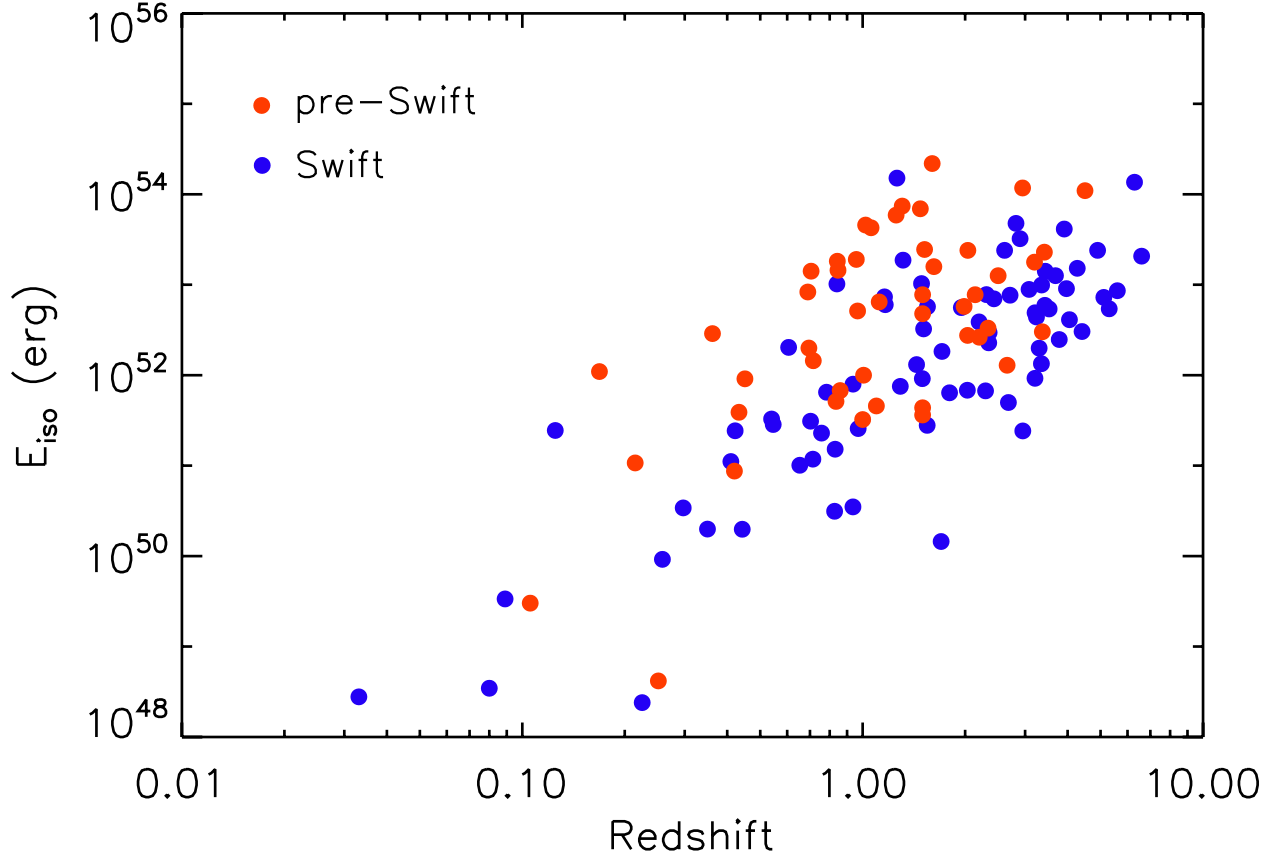


Fig. 3.— A plot of E_{iso} vs. redshift for all detected pre-Swift (red) and post-Swift (blue) events (Long, Short, and SN-associated GRBs). Overall, the Swift detected distribution of E_{iso} extends to lower energies compared to the pre-Swift sample. The apparent correlation is a result of an unknown population evolution combined with detector threshold effects (see Butler, Kocevski, et al. 2007).

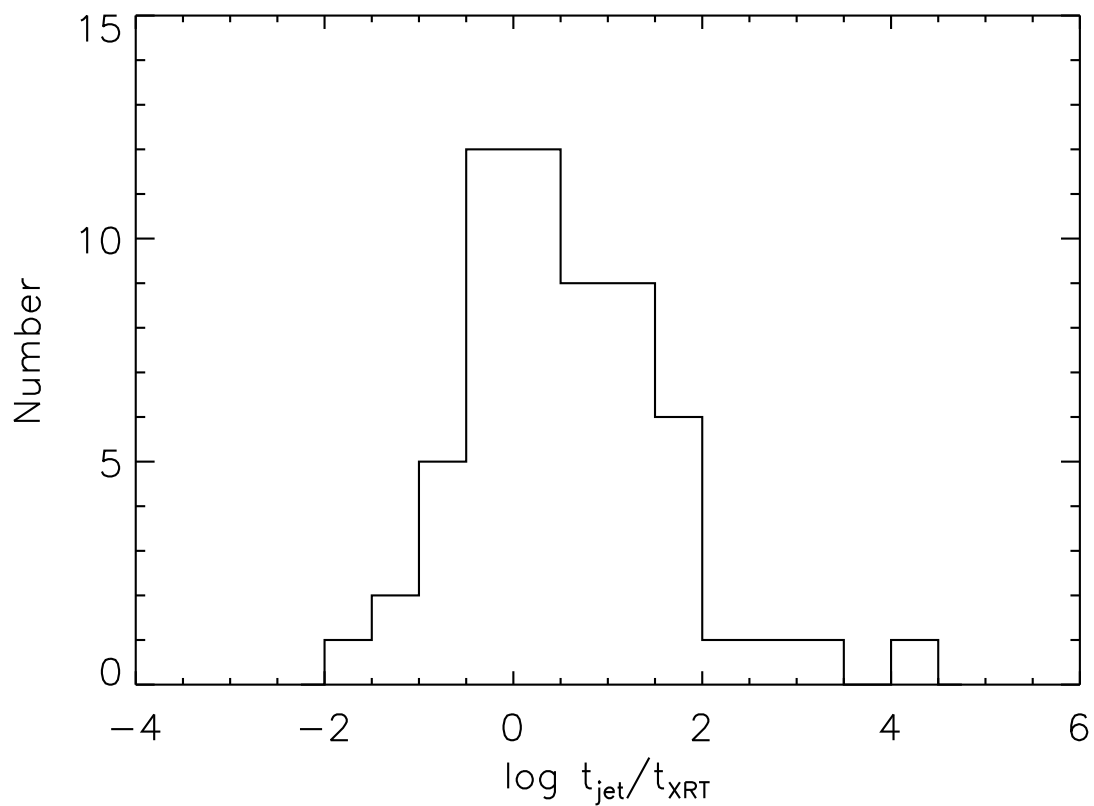


Fig. 4.— A histogram of the ratio between t_{jet} and the last 3σ XRT observation t_{XRT} . Roughly 63% of our LB sample have an expected t_{jet} , when assuming a fixed pre-Swift E_γ , that occurs beyond the last 3σ XRT observation.

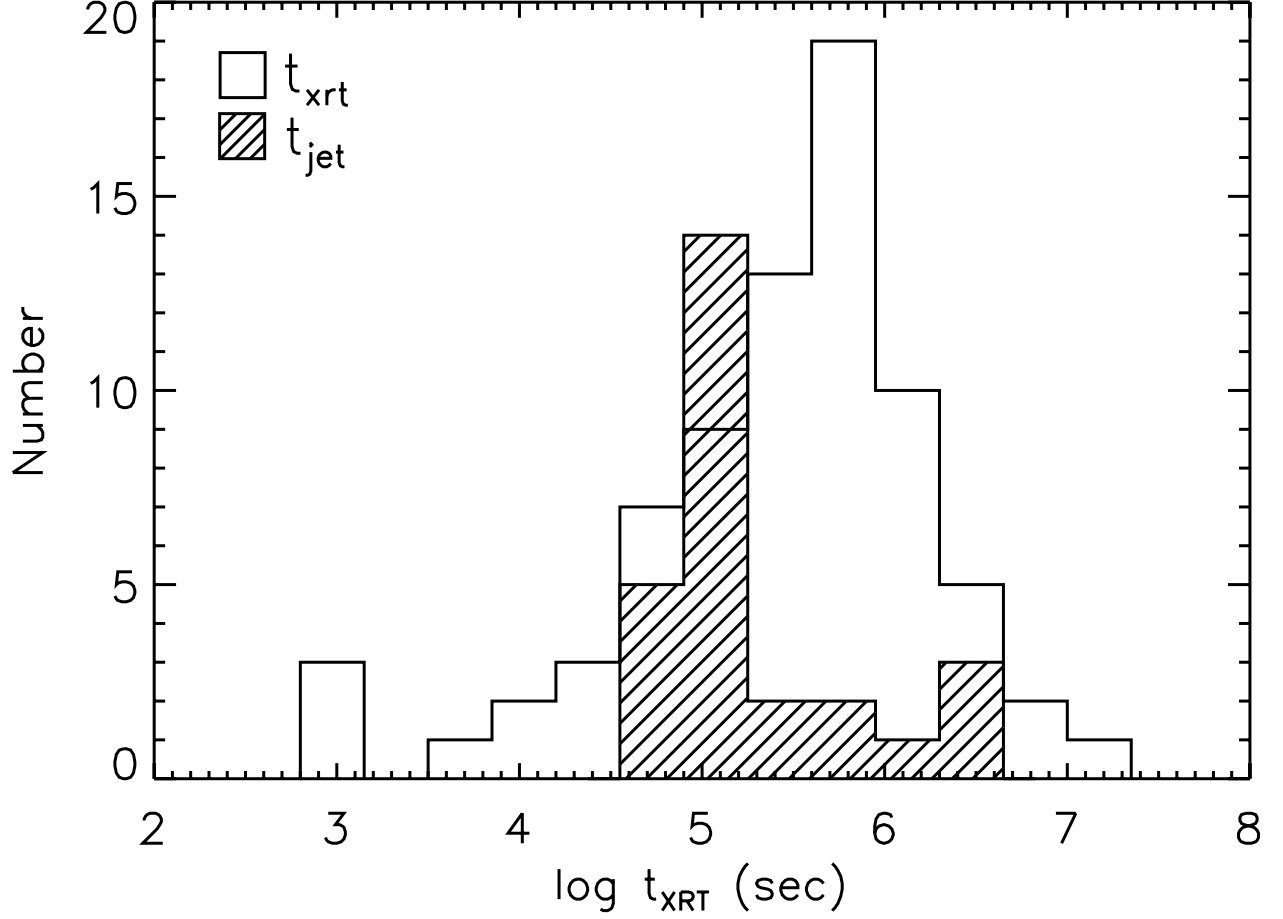


Fig. 5.— A comparison of t_{XRT} for our LB sample to the pre-Swift t_{jet} distribution, with the pre-Swift jet breaks shown as the filled histogram. The median of the two distributions differ by roughly an order of magnitude.

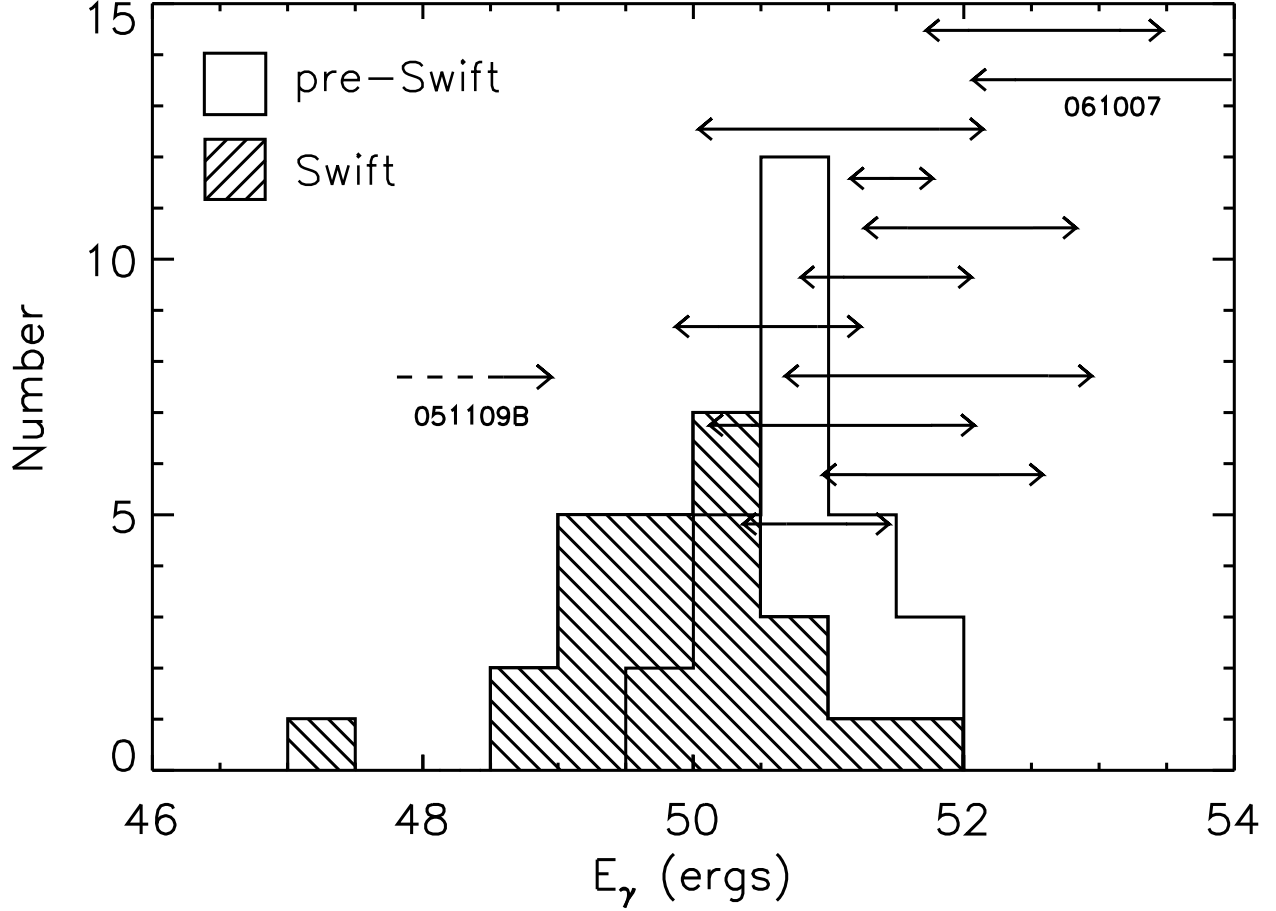


Fig. 6.— A comparison between the pre- and post-Swift collimation corrected energy E_γ as determined through the use of optical and X-ray determined jet break times, respectively. The peak of the post-Swift E_γ distribution is roughly an order of magnitude lower the standard energy derived from the pre-Swift observations. This is due to Swift’s detection of lower energy and higher redshift events as well as the early nature of most X-ray breaks. Events with no detected breaks in their X-ray light curves have limits to their E_γ shown as the vertical bars. The lower limit is set by the last XRT observations whereas the upper limit is the burst’s isotropic equivalent energy E_{iso} . Several events begin to push the post-Swift E_γ distribution beyond 10^{52} ergs.

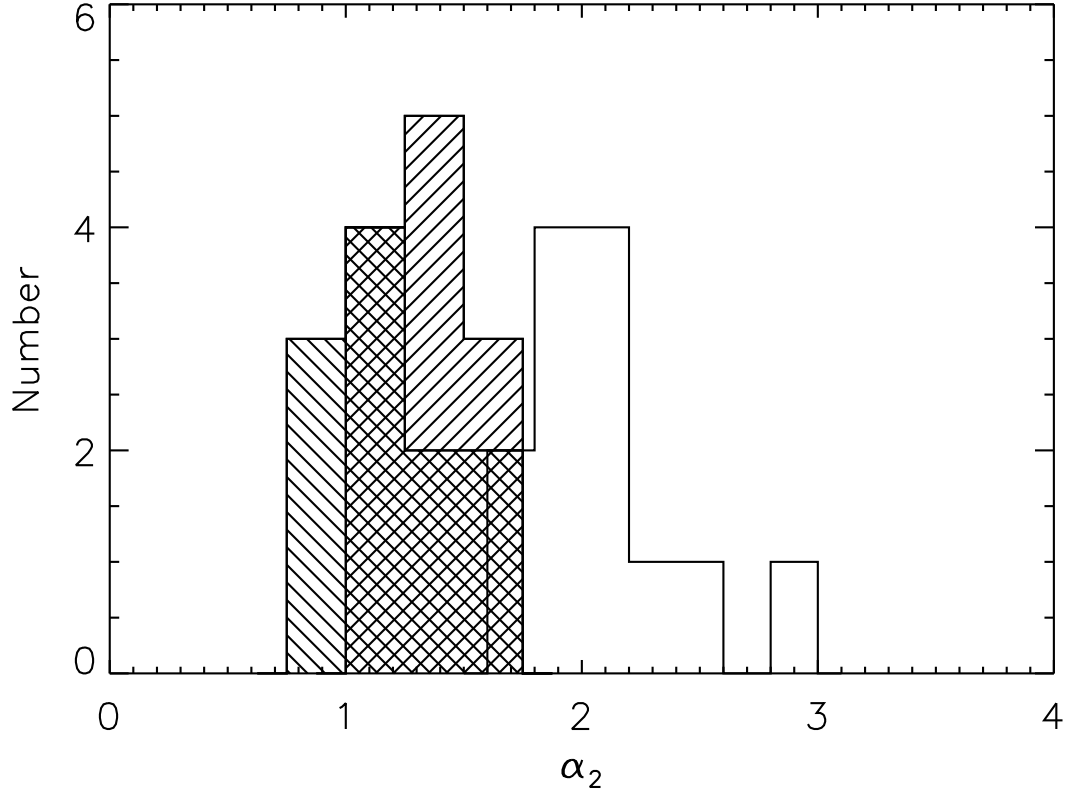


Fig. 7.— A comparison of the post-break decay indices of events containing jet breaks consistent with model predictions (solid histogram) to the post-break decay indices of events containing breaks not fully consistent with jet models (filled histogram at -45°). The final decay indices for the events which show no breaks in their light curves is shown as a filled histogram at $+45^\circ$.

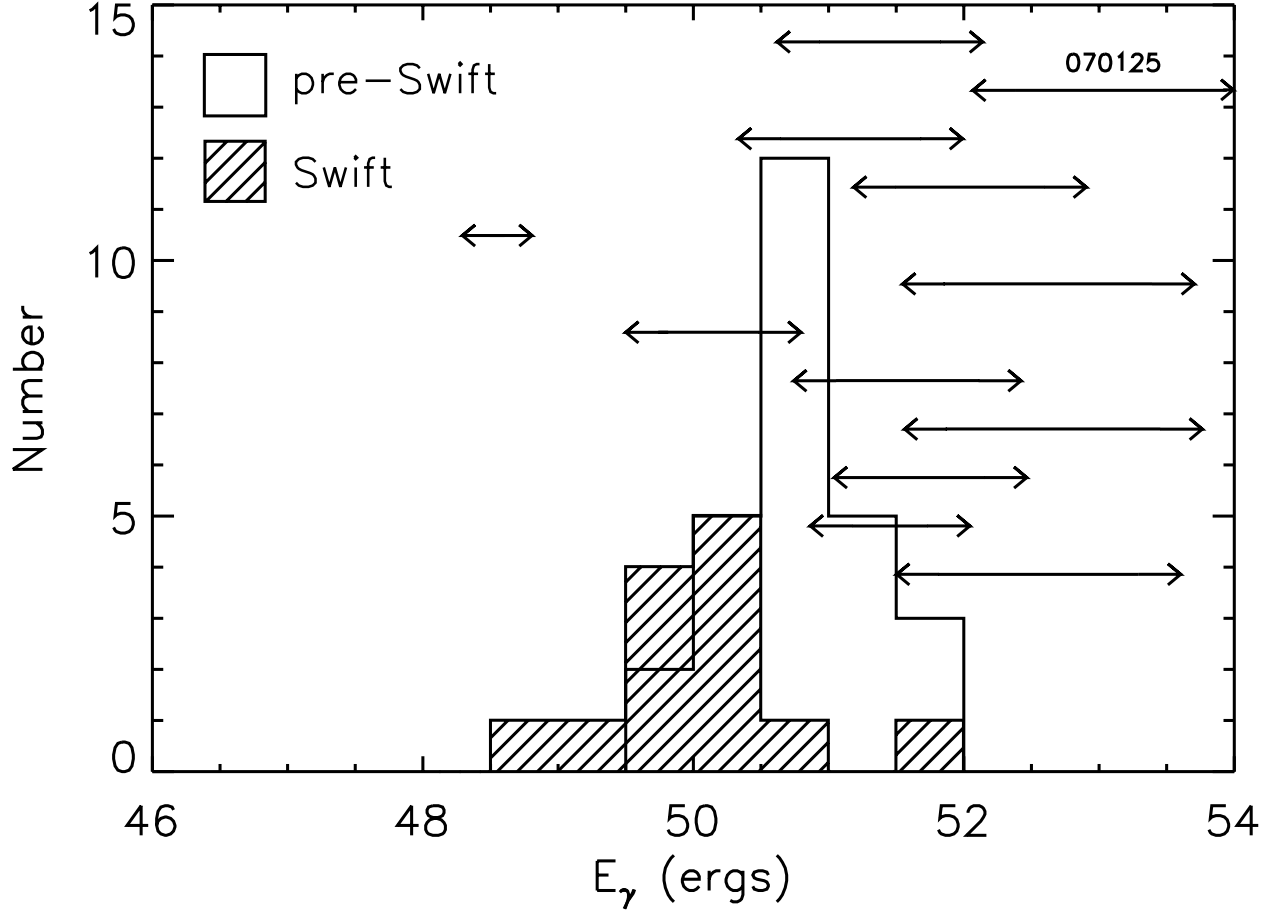


Fig. 8.— Similar to Figure 7, but the events for which the X-ray breaks have a post-break decay that is shallower than $\alpha \sim 1.5$ have been removed from the sample. These breaks do not conform with standard jet model predictions and therefore could be considered suspect. The removal of these events eliminates the low energy tail from the post-Swift E_γ distribution, making it more consistent with the optically determined pre-Swift energetics distribution. The upper and lower limits to the E_γ for these events with shallow breaks are shown as vertical bars. Much like the events with no detected jet breaks, the limits on E_γ for many of these shallow break events are well above the pre-Swift E_γ distribution pushing the upper end of the post-Swift energy distribution well beyond 10^{52} ergs.

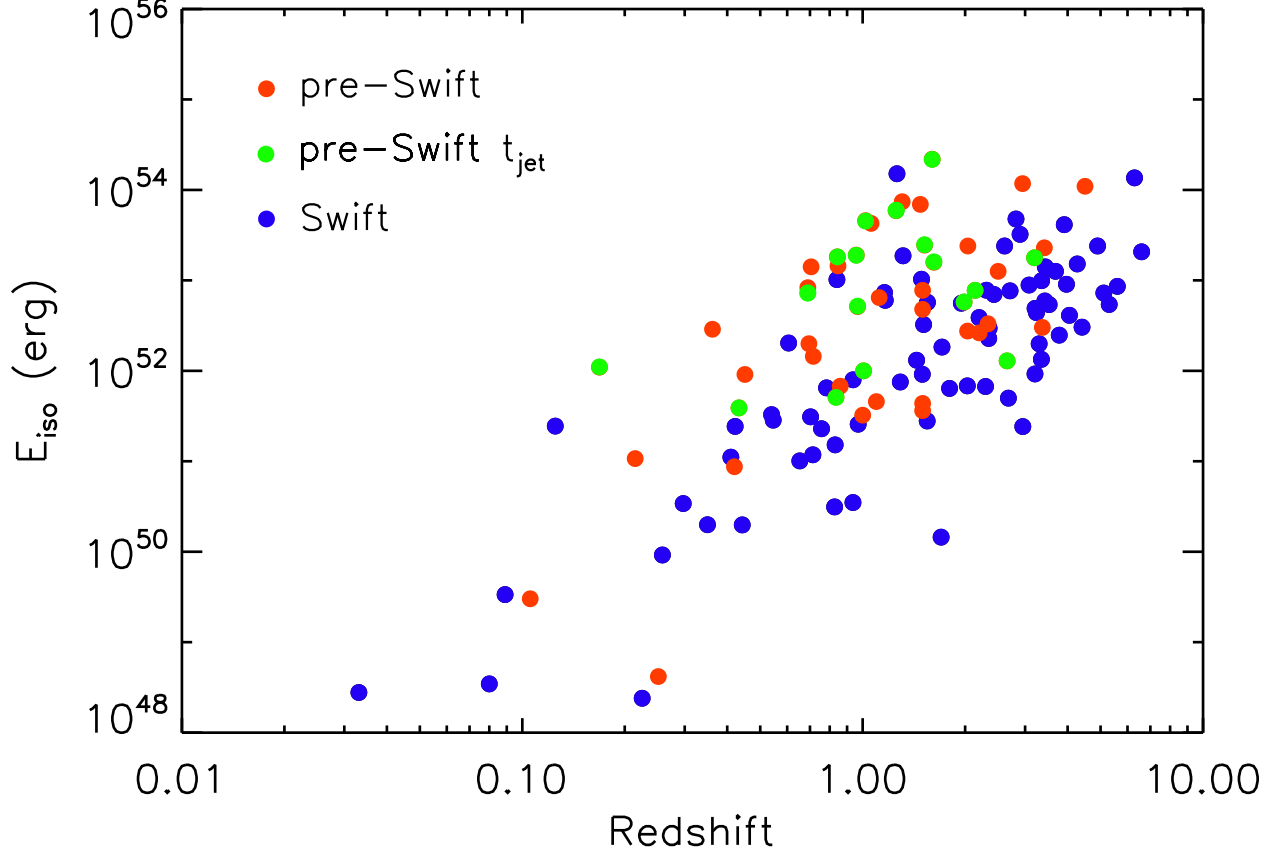


Fig. 9.— A plot of E_{iso} vs. redshift for all detected pre-Swift (red) and post-Swift (blue) events (Long, Short, and SN-associated GRBs). The pre-Swift events for which a jet break was detected are shown in green. These pre-Swift GRBs that contain jet break tend to populate a high E_{iso} and intermediate redshift parameter space. Overall, the Swift detected distribution of E_{iso} extends to lower energies compared to the pre-Swift sample.

Table 1. 76 Swift Detected GRBs With Measured Redshift

GRB ^a	Redshift ^b	$\log E_{\text{iso}}$ (ergs)	$\log t_{\text{XRT}}^{\text{c}}$ (s)	$\log E_{\gamma, \text{XRT}}^{\text{d}}$ (ergs)
050126	1.29*	51.88 (0.13,0.38)	4.77	>51.90
050315	1.95	52.75 (0.00,0.33)	5.98	>53.05
050318	1.44*	52.12 (0.15,0.02)	4.80	>51.88
050319	3.24	52.64 (0.04,0.40)	4.97	>51.25
050401	2.90	53.51 (0.10,0.25)	5.88	>53.67
050416A	0.65*	51.00 (0.11,0.17)	6.81	>51.23
050505	4.27	53.18 (0.10,0.28)	5.70	>53.45
050509B†	0.22	48.38 (0.22,0.46)
050525	0.61	52.31 (0.02,0.02)	6.05	>51.99
050603	2.82	53.68 (0.21,0.27)	5.78	>53.98
050724†	0.26	49.96 (0.10,0.33)	5.26	>49.67
050730	3.97	52.96 (0.16,0.28)	5.68	>53.26
050802	1.71	52.26 (0.09,0.27)	5.90	>52.11
050803	0.42*	51.39 (0.18,0.30)	5.92	>51.51
050813†	1.70	50.16 (0.34,0.44)	3.04	>50.44
050814	5.30‡	52.73 (0.11,0.18)	5.94	>52.39
050820A	2.61	53.38 (0.26,0.25)	6.70	>53.58
050824	0.83	51.18 (0.15,0.82)	6.31	>51.30
050826	0.30*	50.53 (0.36,0.33)	5.40	>49.37
050904	6.29	54.13 (0.17,0.17)	4.73	>54.40
050908	3.35	52.13 (0.12,0.21)	4.97	>51.35
050922C	2.20	52.59 (0.09,0.23)	5.00	>51.87
051016B	0.94*	50.54 (0.06,0.42)	5.73	>50.85
051109A	2.35	52.36 (0.11,0.31)	6.19	>52.33
051109B	0.08*	48.54 (0.11,0.20)	4.92	>46.87
051111	1.55	52.76 (0.12,0.28)	4.67	>52.33
051221A†	0.55	51.45 (0.19,0.24)	5.86	>51.33
051227†	0.71*	51.07 (0.26,0.36)	5.21	>51.34
060108	2.03‡	51.83 (0.13,0.32)	5.53	>51.73
060115	3.53	52.73 (0.03,0.19)	5.67	>52.92

Table 1—Continued

GRB ^a	Redshift ^b	$\log E_{\text{iso}}$ (ergs)	$\log t_{\text{XRT}}^{\text{c}}$ (s)	$\log E_{\gamma, \text{XRT}}^{\text{d}}$ (ergs)
060116	6.60 \ddagger	53.32 (0.16,0.26)	5.20	>53.27
060124	2.30	51.83 (0.11,0.31)	6.28	>51.07
060202	0.78*	51.81 (0.08,0.29)	6.44	>50.62
060206	4.05	52.61 (0.07,0.11)	6.57	>52.89
060210	3.91	53.62 (0.09,0.27)	5.94	>53.90
060218	0.03	48.44 (0.10,0.18)	5.90	>47.66
060223A	4.41	52.48 (0.07,0.15)	4.49	>52.74
060418	1.49	53.01 (0.10,0.23)	5.52	>53.17
060428B	0.35*	50.30 (0.10,0.29)	5.98	>49.81
060502A	1.51	52.51 (0.14,0.27)	6.20	>52.81
060502B \ddagger	0.09*	49.53 (0.33,0.41)	3.15	>49.35
060510B	4.90	53.38 (0.10,0.14)	5.16	>53.21
060512	0.44*	50.30 (0.10,0.40)	5.39	>47.96
060522	5.11	52.86 (0.09,0.29)	5.38	>52.20
060526	3.21	52.69 (0.01,0.34)	5.33	>52.79
060604	2.68	51.70 (0.09,0.53)	5.90	>50.66
060605	3.78	52.39 (0.13,0.35)	4.84	>51.85
060607A	3.08	52.95 (0.08,0.25)	5.30	>52.68
060614 \ddagger	0.12	51.39 (0.09,0.06)	5.85	>51.17
060707	3.43	52.77 (0.06,0.13)	6.23	>52.95
060708	1.80 \ddagger	51.81 (0.09,0.19)	5.80	>51.18
060714	2.71	52.88 (0.05,0.30)	5.81	>51.82
060729	0.54	51.52 (0.08,0.28)	7.12	>51.60
060904B	0.70	51.49 (0.11,0.20)	5.27	>51.76
060906	3.68	53.10 (0.04,0.30)	4.85	>53.17
060908	2.43	52.84 (0.09,0.19)	5.90	>52.53
060912A	0.94*	51.90 (0.14,0.21)	5.39	>51.95
060926	3.21	51.97 (0.09,0.55)	5.06	>51.99
060927	5.47	52.93 (0.07,0.09)	3.79	>52.98
061004	3.30	52.30 (0.06,0.20)	5.17	>52.26

Table 1—Continued

GRB ^a	Redshift ^b	$\log E_{\text{iso}}$ (ergs)	$\log t_{\text{XRT}}^{\text{c}}$ (s)	$\log E_{\gamma, \text{XRT}}^{\text{d}}$ (ergs)
061007	1.26	54.18 (0.24,0.22)	5.78	>54.47
061028	0.76*	51.36 (0.12,0.36)	4.39	>51.01
061110B	3.44	53.15 (0.36,0.31)	4.21	>53.42
061121	1.31	53.27 (0.11,0.21)	6.34	>53.31
061126	1.16*	52.87 (0.15,0.29)	6.13	>52.38
061210†	0.41*	51.05 (0.43,0.35)	5.58	>50.54
061217†	0.83*	50.50 (0.42,0.34)	4.12	>50.18
061222B	3.36	53.00 (0.18,0.19)	4.77	>53.08
070110	2.25	52.47 (0.09,0.27)	6.36	>52.69
070208	1.17	51.45 (0.14,0.26)	5.30	>51.09
070306	1.50*	52.78 (0.08,0.28)	6.06	>50.55
070318	0.84	51.96 (0.12,0.29)	6.00	>52.25
070411	2.95	53.01 (0.09,0.25)	5.84	>53.31
070419A	0.97	51.38 (0.11,0.28)	3.07	>51.44
070506	2.31	51.41 (0.10,0.22)	3.91	>51.47
070508	0.82*	52.89 (0.07,0.08)	5.51	>53.18

^aShort GRBs are denoted by a dagger and are excluded from our primary analysis.

^bPhotometrically determined redshifts are marked with a double dagger. Redshifts determined through host association are denoted with an asterisk. A full reference list for all quoted redshifts can be found in Butler et al. (2007).

^cThe last 3σ detection of the afterglow by the XRT.

^dThe lower limit on E_{γ} when using the last XRT observation as the lower limit to the jet break time.

Table 2. GRBs With Potential Jet Breaks

GRB ^a	Redshift	$\log t_{\text{jet}}$ (s)	α_1	α_2	$\log E_\gamma$ (ergs)
050315	1.95	5.41	0.64	1.91	50.72
050318	1.44	4.41	1.35	2.06	49.56
050319	3.24	4.78	0.67	1.71	50.05
050505	4.27	4.84	1.27	1.90	50.43
050730	3.97	4.11	0.82	2.57	49.73
050803	0.42	4.11	0.29	1.76	48.96
050814	5.30	4.94	0.81	2.24	50.11
051022	0.80	5.41	1.40	2.18	51.54
060526	3.21	5.11	0.89	2.91	50.34
060605	3.78	4.11	1.04	2.10	49.33
060614	0.12	5.11	1.29	2.14	49.79
060906	3.68	4.24	0.43	1.81	49.96
070306	1.50	4.78	1.20	1.91	50.33
...
050401	2.90	3.39	0.66	1.38	49.69
050408	1.24	4.55	0.70	1.00	49.50
050525A	0.61	3.78	0.91	1.39	49.37
050603	2.82	4.83	1.40	1.70	50.90
050802	1.71	3.81	0.73	1.25	49.18
051016B	0.94	4.80	0.80	1.17	48.74
060210	3.91	4.67	0.98	1.28	50.65
060218	0.03	4.73	0.82	1.23	47.32
060707	3.43	4.72	0.60	1.05	50.09
060708	1.80	4.20	0.74	1.38	49.13
070125	1.55	5.11	0.90	1.60	51.49
070318	0.84	5.44	1.17	1.71	50.31

^aThe first group consists of GRBs with spectral and temporal behavior found by Panaitescu (2007a) to be consistent with standard jet models. The second group have light curve breaks that are not fully consistent with model predictions, but have exhibit steepening that resembles jet break behavior.

